A Novel Sediment Transport Model (STM) Accounting Phase Lag Effect. A Resonance Condition.

ARNO ROLAND NGATCHA NDENGNA[1], YVES MIMBEU[1], RAPHAEL ONGUENE[2], SÉVÉRIN NGUIYA[1], ABDOU NJIFENJOU[1,3]

[1]E3M Laboratory, National Higher Polytechnic School of Douala,
University of Douala,
P.O.BOX 2701, Douala,
CAMEROON

[2]Laboratory of Technology and Applied Science,
University of Douala, Douala,
CAMEROON

[3]Department of Mechanical Engineering,
National Advanced School Polytechnic, University of Yaoundé I,
P.O.BOX 8390, Yaoundé,
CAMEROON

Abstract: - The classical Exner model coupled with a bed-load sediment flux formula is widely used to describe the morphodynamics of coastal environments. However, the main drawbacks of this model are (i) Lack of robustness, (ii) Lack of differentiation between sediment and fluid velocities, and (iii) Generation of instabilities when the interactions between sediment and fluid flow become more important. Moreover, Exner's model does not allow us to know with which characteristic velocity the bottom is moving. This set of drawbacks weakens the effectiveness of most sediment transport models proposed in the literature, particularly the Exner model. In this work, we reformulate the bed-load equation and we propose a new averaged sediment transport model for application in coastal or estuarine environments. The proposed model incorporates phase shift effects into the bed-load equation. The bedform's characteristic velocity, sediment, and fluid velocity are differentiated. We developed a new first-order, well-balanced, positivity-preserving, path-preserving, and central wind (WBPP-PCCU) scheme to solve the proposed hyperbolic sediment transport model (HSTM). We used the Averaging Essentially Non-Oscillatory (AENO) reconstruction coupled with the third-order Runge-Kutta Semi-Implicit (SI-RK3) method to achieve second-order accuracy. The balance and positivity of the water depth properties were proven. In this work, a resonance condition is proposed. The model facilitates the application of several other schemes such as Roe, HLLC, HLLEM, PVM (polynomial viscosity matrix), RVM (rational viscosity matrix), which require the diagonalization of the Jacobian matrix. The accuracy, robustness, positivity preservation, and equilibrium properties of the resulting model are evaluated using a series of carefully selected test cases. The proposed model provides an excellent ability to simulate sediment transport in a wide range of coastal environments.

Key-words: - Hyperbolic Sediment Transport Model (HSTM), Phase lag effects, Resonance condition, Path-Conservative Central-Upwind (PCCU) scheme, Well-Balanced Preserving-Positivity, (WBPP), AENO reconstruction, Coastal environment.

Received: July 22, 2021. Revised: October 8, 2022. Accepted: November 11, 2022. Published: December 16, 2022.

1 Introduction

When a fluid moves over a mobile bedform, a buoyant force, which tends to lift the sediments from its bed, appears. Under the action of their weight (depending on their density or size), they may fall (sedimentation), or under the action of the turbulence, they may remain in motion (or in suspension) and then be transported by the current (erosion) or by a combined action of the current and waves. The number of grains eroded from the

bed load per unit area and time is also defined as the pick-up rate. A coastal zone frequently adjusts its cross-section, longitudinal profile, course flow, and pattern through the processes of scouring deposition, which hinders the optimal operation of seaports. Two main modes of transport are therefore highlighted: (i) The transport by suspension of sediments above the bottom or on the boundary layer, (ii) the bed-load transport of the same that have fallen to the bottom. We recall that sediment transport occurs when the bottom stress is slightly above the threshold. The bed load transport is difficult to predict due to the presence of some physical and hydrodynamic parameters complicated to model.

These parameters that influence the bedload sediment transport processes have been studied by some authors: Cannata *et al*, [1], Chengini and Pender, [2], Exner, [3], Greimann and Huang, [4], Tassi and Villaret, [5], Vah *et al*, [6], Rijn, [7], Rijn *et al*, [8], Soulsby, [9]. These parameters are of interest to geomorphology. Some among them (such as phase lag and shear) are often neglected in several coastal engineering applications. To investigate sediment transport with accuracy, these parameters are necessary. Accounting for these parameters can improve the prediction of flood inundation for insistence. The prediction of dam-break flows over erodible sediment requires an velocity, fluid velocity, and sediment velocity.

The proposed model is less time-consuming and can compete with those using two-phase equations, [12]. Generally for some fully coupled STM, it is more expensive and complicated to find the eigenvalues and eigenvectors (loss hyperbolicity) due to the presence of several coupled terms. The lack of hyperbolicity can create some numerical difficulties. A numerically suitable Alternative is to formulate a bed-load equation in which the characteristic velocity $u_b\left(Z_b\right)$ (see Fig.1) of the bedform is given as a function of the depth average of the flow and sediment characteristics (as the Froude number Fr)

$u_b\left(Z_b\right)=f\left(Fr,p,u_s\right)$.

p and u_s being the bed porosity and the sediment velocity respectively.

important choice of the bed-load equation for morphodynamics. For example, when the sediment size becomes greater, exaggerated inaccurate results can appear and even produce a non-realistic description of the dynamics of the sediment bed. Several sediment transport models require some sediment flux formula as the well-known Grass formulae, [10]. Meyer-Peter & Muller (MPM), Nielsen, and Van Rijn formulas (see [9]) can be written in the form of Grass-type by adapting the constant depending on experimental data and taking into account the grain diameter and the kinematic viscosity. All the Grass-type formulas assume that the motion begins at the same time for the fluid and the sediment. This assumption is not realistic in some practical cases. The sediment transport includes the dynamics of the water flow modeled by Shallow Water Equations (SWE), [11], widely studied in the literature in Cartesian, [12], [13], [4], [14], [15] and in curvilinear coordinates [16]. Sediment transport models based on SWE and Exner-based models ignore the phase lag effect and cannot give us the characteristic velocity with which the bottom moves. The sediment time is greater than the hydrodynamic time. Thus dynamics of the water and the dynamic of sediment must be studied using a mathematical model. Differentiating the bedform's characteristic

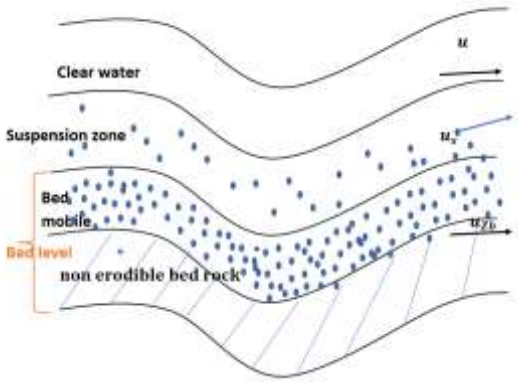

Fig. 1: Physical description of the model.

The model admits an easy-to-find eigenstructure without using the Lagrange theorem as in, [17], or Gerschgorin as in, [18], or a splitting technique as in Siviglia *et al*, [19], Ngatcha *et al*, [20]. The implementation of the Lagrange or Gerschgorin theorems is not easy and requires several considerations. Additionally, for some sediment transport problems, the splitting technique can fail. Therefore the model is hyperbolic (eigenvectors and eigenvalues are easily computed) and a wide range of existing numerical methods in the

literature without major difficulties. Hyperbolicity ensures the existence of a numerical solution.

Some numerical schemes have been used to solve the sediment transport equations, [13], [21], [1], [22] [23], [24], [25], [26], [27]. Computer software could be very helpful to understand both hydrodynamics and morphodynamics. The STM is nonconservative and must be solved by using a nonconservative scheme. The above schemes do not apply to several sediment transport problems. One of the causes of these shortcomings is the presence of nonconservative terms and many coupled terms. The proposed model is solved by the finite volume methods in path-conservative frameworks. The concept of path conservative developed by Parès, [28], is based on the nonconservative product theory of Dal Maso-Lefloch-Murrat, [29]. This numerical method is widely used to design suitable numerical schemes for solving sediment transport problems, [14], [19], [30]. Another objective of this study is to develop a high-order resolution well balanced and positive numerical method to approximate solutions to sediment transport problems. We aim to extend the path-conservative central-upwind scheme (referred to as the PCCU scheme) originally developed by Castro *et al*, [31], for solving fully coupled STM. The classical well-balanced PCCU scheme turns out to be limited for sediment transport problems. This scheme has been used to solve SWE by Castro *et al*, [31], the Saint-Venant-Exner model by Ngatcha *et al*, [14], and Ngatcha *et al* s model, [32]. The PCCU scheme is seen as a version of the path-conservative HLL scheme of Dumbser and Basalra, [33], or of the path-conservative HLL of Xin [34].

A major difficulty in developing the PCCU or path-conservative HLL schemes isrelated to the numerical computation of steady-state and quasi-steady-state solutions. It's important to design a numerical method that verifies the C-property. A well-balanced discretization strategy developed in, [14], is used here without major modifications. The scheme is also positive i.e. preserves the positivity of the water depth.

The first objective of this paper is to propose a new sediment transport model that accounts for special properties. The model consists of SWE with density variation and sediment exchanges, a suspension equation, and finally an equation that describes the motion of the bottom. The model is simple and is seen as an improvement of existing sediment transport models based on classical Exner equations such as, [23], [35], [24]. With this special bed-load equation, it's possible to identify the hypersurface on which some waves have the same characteristic fields.

The goal of this paper is to propose a second-order well-balanced positivity preserving PCCU scheme to solve the model. To design this scheme, we adopt a version of the AENO (Averaging Essentially Non-Oscillatory) procedure originally developed by Toro *et al*, **[36]** and applied for the first time in Ngatcha and Njifenjou, **[14]**. We have used a strategy of time-discretization based on the Semi-Implicit third-order Runge-Kutta (SI-RK3) method of Chertock et al, **[37]** to solve the problem related to friction which is another difficulty of the present model. The resulting fully discrete second-order scheme is well-balanced, positive, stable, accurate, robust, and non-oscillatory and can be extended to a class of nonconservative problems.

The rest of the paper is presented as follows. Section (2) is dedicated to introducing the mathematical model that couples the generalized Saint-Venant equations, bed-load equation, and sediment transport equation. The hyperbolicity study of the system is also proposed. In section (3) the semi-discrete first-order PCCU scheme is exposed. Section (4) presents the second-order well-balanced preserving-positivity scheme. In section (5), some tests are made and the numerical results are compared and discussed. Section (6) presents some conclusions and remarks.

2 Mathematical Model and Properties

2.1 Governing Equations

The starting point is the 2D evolution equations of mixing fluid dynamics and sediment volume rate. These equations describe the evolution of fluid mixing in a domain bounded by a dynamic water surface and water bed. Taking into account the kinematic conditions on the moving surfaces, we apply an average along the depth of the equations to obtain simplified equations (shallow water equation in Cartesian coordinates)**.** We also can use the integral form of contravariant shallow water equations in the one-dimensional curvilinear coordinate system, [16]. We take an Eulerian approach for the sediment transport equations. The sediment transport model proposed here reads:

$$\begin{aligned}
&\frac{\partial h}{\partial t}+\frac{\partial hu}{\partial x}=\frac{E-D}{(1-p)}\\
&\frac{\partial hu}{\partial t}+\frac{\partial}{\partial x}\left(huu+\frac{1}{2}gh^2\right)+gh\frac{\partial Z_b}{\partial x}+\frac{(\rho_s-\rho_w)}{2\rho}gh^2\frac{\partial C}{\partial x}=-C_f|u|u-\frac{(E-D)}{(1-p)}\mathrm{u}\\
&\frac{\partial (hC)}{\partial t}+\frac{\partial (huC)}{\partial x}=\frac{\partial}{\partial x}\left(f_s h\nu_m\frac{\partial C}{\partial x}\right)+(E-D)\\
&\frac{\partial Z_b}{\partial t}+u_b(Z_b)\frac{\partial (Z_b)}{\partial x}=-\frac{E-D}{(1-p)}
\end{aligned} \tag{1}$$

Here, $h[m]$ is the water depth, $u[m/s]$ is the averaged x-velocity, $hu=q[m^2/s]$ is the water discharge, $Z_b[m]$ and is the bed level. $g[m/s^2]$ is the gravity constant.

The friction source term is given by manning's laws $C_f=n^2gh^{-1/3}$,

$n[s/m^{1/3}]$ being manning's coefficient. Generally, this coefficient depends on the bed sediment distribution. All these parameters can be seen in Fig. (2).

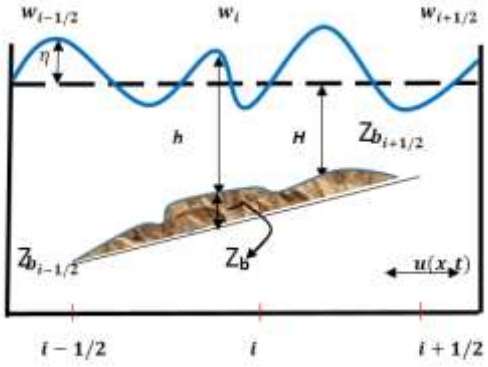

Fig. 2: Physical and hydrodynamic parameters

There is a counterpart in the evolution of the fluid volume fraction that will compensate to achieve the following evolution of the mixture density:

$$\rho=\rho_w(1-C)+\rho_s C, \tag{2}$$

where $\rho_w,\rho_s[Kg/m^3]$ and C is the water density, sediment density, and averaged sediment concentration volumetric respectively. The pressure here is considered hydrostatic. But we also can consider the non-hydrostatic part of pressure as in, [38]. f_s is the transport mode parameter representing the suspended load fraction as introduced by Greimann and Huang, [4] (see appendix A). The suspension is sufficiently dilute (Boussinesq approximation) to consider that the value of the kinematic viscosity of water/sediment ν_m is equal to the corresponding clear water.

Different modes of suspensions can be integrated into the governing equations: frozen particles mode, when $u_s=u$ (u_s solid velocity) asymptotically, and the filtering particles mode, when $u_s\neq u$. In all cases, the size of particles is much less than the distances between the nearest particles. However, the suspension equations describing the asymptotic behavior of the solution when the diameters of particles and the distances between neighbors tend to zero can be given by a homogenization approach. Here for sake of simplicity, only the case when the velocities of particles coincide (asymptotically) with the averaged fluid velocity is considered.

$E,D[Kg/m^2/s]$ are the erosion and deposition we detail in appendix A (see also [8]). Here, we have approximated the sediment flux by $u_b(Z_b)\frac{\partial Z_b}{\partial x}$ where $u_b(Z_b)=u_b$ is the characteristic velocity of the bedform given by:

$$u_b=\frac{1}{(1-p)}\frac{1}{(1-Fr^2)}\frac{u_s}{|u|} \tag{3}$$

where p is the sediment bed porosity, $u_s=C_s u$ is the averaged sediment velocity, and C_s is a positive calibration parameter and where

$Fr = \dfrac{|u|}{\sqrt{gh}}$ is the Froude number. It's important to remark on that $u_b(Z_b) \neq u_s \neq u$. The new bed-load model given by the last equation of Eq. (1) and Eq. (3) permits us to take into account the phase lag effect. The characteristic velocity of the bedform depends on sediment velocity, bed porosity, and of the Froude number. Therefore, the movement of the bedform is directed by the regime of flow.

Remark Here, the mass conservative of moving particles and boundary conditions at the bed interface are used for the modeling of the bed-load sediment transport. The bed boundary is viewed as a phase interface across which the fluid/sediment mixture undergoes a transition from solid to fluid-like behavior.

2.2 Generalized Jump Conditions (R-H Relations)

In the following, we will assume that W^+, W^- the right and left state is a Riemann problem. Let us define the average and jump operators by: $[\![.]\!] = (.)_+ - (.)_-$ and $\{\{.\}\} = \dfrac{(.)_+ + (.)_-}{2}$. The Rankine-Hugoniot condition reads:

$$[\![hu]\!] = \sigma [\![h]\!],$$

$$\left[\!\!\left[hu^2 + \frac{1}{2}gh^2\right]\!\!\right] + g\{\{h\}\}[\![Z_b]\!] + g\frac{\delta\rho}{2\rho}\{\{h^2\}\}[\![C]\!] = \sigma [\![hu]\!],$$

$$[\![huC]\!] = \sigma [\![hC]\!],$$

$$\{\{u_b\}\}[\![Z_b]\!] = \sigma [\![Z_b]\!].$$

Here, σ is a jump of discontinuities $\overline{\rho} = \{\{\rho\}\}$.

where S_F, S_e, S_D are the friction source term, the sediment exchange source term, and the diffusion source term. These terms write:

$$S_F = \begin{pmatrix} 0 \\ -C_f |u| u \\ 0 \\ 0 \end{pmatrix},$$

$$S_e = \begin{pmatrix} \dfrac{E-D}{1-p} \\ -\dfrac{(E-D)u}{(1-p)} \\ E-D \\ -\dfrac{E-D}{1-p} \end{pmatrix}, \quad S_D = \begin{pmatrix} 0 \\ 0 \\ \dfrac{\partial}{\partial x}\left(f_s h \nu_m \dfrac{\partial C}{\partial x}\right) \\ 0 \end{pmatrix}$$

An admissible space can be given by $\Omega^0 = \{W \in \mathbb{R}^4, h > 0\}$.

This model is a quasi-linear nonconservative system of equations admitting non-trivial steady-state solutions that often carry important physical meaning. Solving this system requires a particular numerical method exposed below.

2.3 Hyperbolicity Study

Let us use the conservative variable and rewrite Eq. (1) in non-conservative form as:

$$\frac{\partial W}{\partial t} + \frac{\partial F(W)}{\partial x} + B_1^*(W)\frac{\partial Z_b}{\partial x} + B_{2c}^*(W)\frac{\partial hC}{\partial x} + B_{2h}^*(W)\frac{\partial h}{\partial x} = \hat{\mathbf{S}}(W); \quad x \in \Omega \subset \mathbb{R}, \quad t \in (0,T)$$

The system is equipped with boundary and initial conditions.

The physical flux vector is given by

$$F(W) = \begin{pmatrix} hu \\ huu + 0.5gh^2 \\ huC \\ 0 \end{pmatrix},$$

the source term $\hat{\mathbf{S}}(W) = S_e + S_F + S_D$

The nonconservative vectors are:

$$B_1^* = \begin{pmatrix} 0 \\ gh \\ 0 \\ u_b \end{pmatrix}, \quad B_{2h}^* = \begin{pmatrix} 0 \\ -\dfrac{\delta\rho}{2\rho} ghC \\ 0 \\ 0 \end{pmatrix},$$

$$B_{2C}^* = \begin{pmatrix} 0 \\ \dfrac{\delta\rho}{2\rho} gh \\ 0 \\ 0 \end{pmatrix}, \quad B_2^* = B_{2h}^* + B_{2C}^*.$$

The Jacobian matrix of the LHS of the system reads:

$$\mathrm{A}(W)=\begin{pmatrix} 0 & 1 & 0 & 0 \\ -u^2+gh+\dfrac{\delta\rho}{2\rho}ghC & 2u & -\dfrac{\delta\rho}{2\rho}gh & gh \\ -uC & C & u & 0 \\ 0 & 0 & 0 & u_b \end{pmatrix} \qquad (5)$$

where $\delta\rho=(\rho_s-\rho_w)$

The system is strictly hyperbolic because has four distinct eigenvalues:

$$\lambda_1=u_b,\ \lambda_2=u,\ \lambda_{3,4}=u\pm\sqrt{gh} \qquad (6)$$

The eigenvectors for associated eigenvalues read:

$$E_1=\begin{pmatrix} 1 \\ -u_b \\ C \\ gh-(u-u_b)^2 \end{pmatrix},\ E_2=\begin{pmatrix} \dfrac{\delta\rho}{2\rho} \\ \dfrac{\delta\rho}{2\rho}u \\ \dfrac{\delta\rho}{2\rho}C-1 \\ 0 \end{pmatrix},\ E_3=\begin{pmatrix} 1 \\ u-\sqrt{gh} \\ C \\ 0 \end{pmatrix},\ E_4=\begin{pmatrix} 1 \\ u+\sqrt{gh} \\ C \\ 0 \end{pmatrix} \qquad (7)$$

Recall that the characteristic is genuinely nonlinear in Ω^0

$\nabla\lambda_k(W).E_k(W)\neq 0,\quad \forall\ W\in\Omega^0$.

Or linearly degenerate if

$\nabla\lambda_k(W).E_k(W)=0,\quad \forall\ W\in\Omega^0$

Ω^0 being an admissible space on which the system is hyperbolic. The third and fourth eigenvalues ($\lambda_{3,4}$) correspond to genuinely non-linear characteristic fields in the sense of Lax. While remaining eigenvalues correspond to linearly degenerate characteristic fields be satisfied. This eigenstructure is similar to the one found by Benkhaldoun *et al*, [21].

However, the situation is very different due to the resonance that may appear. Note that under a particular condition, the resonance appears and modifies the characteristic fields of the waves. The admissible waves for the system (1) are the following ones: Rarefaction waves, which are smooth solutions of (1), stationary waves which have zeros speed and satisfy R-H relations when $W^+-W^-=0$, shock waves which satisfy the Rankine-Hugionot relations given above. Under some conditions, all the wave solutions can be obtained by weak formulation. Such a condition may be the occurrence of the resonance phenomenon.

2.4 The Apparition of Resonance Phenomenon

Internal waves trapped by the topography can have a significant effect on local flow dynamics. This effect can be expected to increase the velocity of the fluid near the bottom and thus increase the Shields parameter. Therefore, it can be suggested that the internal waves influence sediment transport and may participate in the formation of sand waves. With this model, we will observe a unique series of resonant internal waves under some conditions. Note that resonant waves may be important in understanding the flow dynamic over the sediment bed. From the eigenstructure of the proposed model, we can see that the conditions for resonance are satisfied if the free internal wavelength that satisfies the unforced equations coincides with the wavelength of topography forcing. This situation appears in our case when:

$$(u-u_b)^2=gh,\ \text{in}\quad \Omega^0 \qquad (8)$$

It's convenient to set

$$\mathrm{C}=\left\{W\in\Omega^0,\ (u_b-u)^2=gh\right\}$$

which is the hypersurface on which all the characteristic fields linearly degenerate. Therefore, the proposed model can predict bed evolution even in the presence of resonance phenomena. In fact, during evolution, a wavelength can be observed in the topography between some distances. In the case of floods with sediment transport, for example, resonance situations could occur only when the flood decelerates slowly.

Remark 1

In the presence of resonance, the above system can be weakly hyperbolic and, in this case, all the eigenvectors are linearly dependent. Under resonance conditions, all the wave solutions can be seen as limited traveling wave solutions.

Remark 2

For 1D and 2D cases, where the classical Exner equation with Grass formula is used, the computationally expensive process of finding all of the eigenvalues of the Jacobian matrices (the upper/lower bounds on the largest/smallest local speeds of propagation) can be avoided: using the Lagrange theorem as in Xin *et al*, [17]. Here, using the novel bed evolution equation proposed above, we compute easily the upper/lower bounds on the largest/smallest local speeds of propagation without using Lagrange or Gerschgorin theorems.

Remark 3

Next, we develop a first-order PCCU scheme. This situation can refer to cases when the solution is piecewise constant. The flux of the proposed semi-discrete scheme is given in the CU sense.

3 New First Order Path-Conservative Central-Upwind (PCCU) Scheme

The grid considered here is uniform that is $K_i = \left[x_{i-1/2}, x_{i+1/2}\right]$, where its measure is the small spatial scale (see Fig. 2).

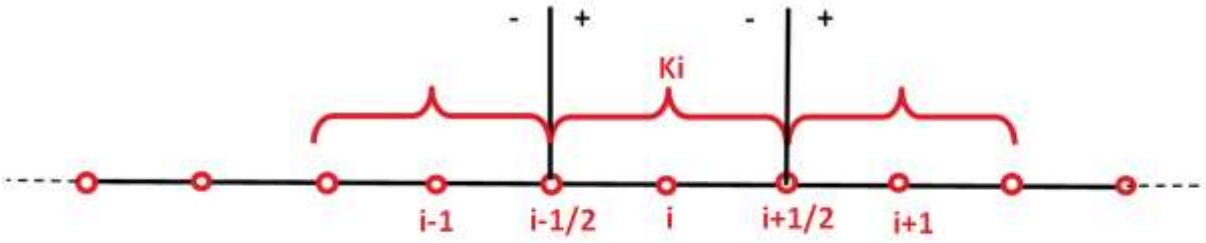

Fig. 3: Finite volume discretization. Cell-centered mesh.

The scheme uses a concept of coupling path-conservative methods and central-upwind techniques. In which the nonconservative terms are integrated directly into the discrete formulation. To design the PCCU scheme, first, we write the central-upwind (CU) scheme for the proposed model. Second, we rewrite the CU scheme of [39] in a path-conservative form (where the fluctuations do not integrate the nonconservative contributions). We will show how the CU scheme does not integrate non-conservative terms. That confirms the fact that the CU scheme (that is exactly the semi-discrete version of the HLL scheme introduced in, [26]) does not apply to non-conservative problems. Here, the fluctuations (denoted $D^{\pm}\left(W^{+},W^{-}\right)$) represent the differences between the numerical flux and the physical fluxes at both sides of the cell interfaces are written only with the derivative of the physical flux $F(W)$. Note that these fluctuations can also be computed by using matrices $\mathrm{A}^{\pm}\left(W^{+},W^{-}\right)$. that D^{-} contribute to the cell K_i and the other D^{+} to the cell K_{i+1}. Next, we integrate the non-conservative terms into the fluctuation without major difficulties. The PCCU scheme resulting can be seen as a version of the path-conservative HLL schemes of Balsara and Dumbser, [33]. Integrating Eq. (4) over the cell K_i, we arrive at the first-order semi-discrete PCCU scheme:

$$\frac{d\overline{W}_i}{dt} = D^{-}_{i+1/2} + D^{+}_{i-1/2}$$

$$= -\frac{1}{\Delta x}\left[\mathrm{F}_{i+1/2} - \mathrm{F}_{i-1/2} - B^{*}_{1,i} - B^{*}_{2,i} + \frac{a^{+}_{i+1/2}}{a^{+}_{i+1/2} - a^{-}_{i+1/2}}\left(\left(B^{*(2)}_{1}\right)^{\Psi}_{i+1/2} + \left(B^{*(2)}_{2}\right)^{\Psi}_{i+1/2}\right) - \frac{a^{-}_{i+1/2}}{a^{+}_{i+1/2} - a^{-}_{i+1/2}}\left(\left(B^{*(2)}_{1}\right)^{\Psi}_{i-1/2} + \left(B^{*(2)}_{2}\right)^{\Psi}_{i-1/2}\right)\right] + S_i \,, \tag{9}$$

which stands for the average value while representing the conservative numerical flux across the interface $x_{i+1/2}$. $B_{1,i}^*$, $B_{2,i}^*$ are the volume contributions of nonconservative terms on cell, $\left(B_1^{*(2)}\right)_{i+1/2}^{\Psi}, \left(B_2^{*(2)}\right)_{i+1/2}^{\Psi}$ are the nonconservative numerical flux. Here, the numerical fluxes $\mathrm{F}_{i+1/2}$ given in a CU flux version reads:

$$\begin{aligned}\mathrm{F}_{i+1/2} &= \frac{a_{i+1/2}^{+}F(W_{i+1/2}^{-})-a_{i+1/2}^{-}F(W_{i+1/2}^{+})}{a_{i+1/2}^{+}-a_{i+1/2}^{-}}+\frac{a_{i+1/2}^{+}a_{i+1/2}^{-}}{a_{i+1/2}^{+}-a_{i+1/2}^{-}}\left(W_{i+1/2}^{+}-W_{i+1/2}^{-}\right)\\ &= \frac{a_{i+1/2}^{+}}{a_{i+1/2}^{+}-a_{i+1/2}^{-}}F(W_{i+1/2}^{-})-\frac{a_{i+1/2}^{-}}{a_{i+1/2}^{+}-a_{i+1/2}^{-}}F(W_{i+1/2}^{+})-\frac{1}{2}\left(\frac{-2a_{i+1/2}^{+}a_{i+1/2}^{-}}{a_{i+1/2}^{+}-a_{i+1/2}^{-}}\left(W_{i+1/2}^{+}-W_{i+1/2}^{-}\right)\right)\end{aligned} \tag{10}$$

$$\begin{aligned}\left(B_1^{*(2)}\right)_i &= \int_{K_i}\left(B_1^{*(2)}\right)\left(\mathbf{P}_i(x)\right)\left(\frac{dP_i^{(1)}}{dx},\frac{dP_i^{(2)}}{dx},...,\frac{dP_i^{(N)}}{dx}\right)^T dx,\\ \left(B_{2,h,C}^{*(2)}\right)_i &= \int_{K_i}\left(B_{2,h,C}^{*(2)}\right)\left(\mathbf{P}_i(x)\right)\left(\frac{dP_i^{(1)}}{dx},\frac{dP_i^{(2)}}{dx},...,\frac{dP_i^{(N)}}{dx}\right)^T dx\end{aligned} \tag{11}$$

$$\begin{aligned}\left(B_1^{*(2)}\right)_{i+1/2}^{\Psi} &= \int_0^1\left(B_1^{*(2)}\right)\left(\Psi_{i+1/2}(s)\right)\left(\frac{d\psi_{i+1/2}^{(1)}}{ds},....,\frac{d\psi_{i+1/2}^{(N)}}{ds}\right)^T ds,\\ \left(B_{2,h,C}^{*(2)}\right)_{i+1/2}^{\Psi} &= \int_0^1\left(B_{2,h,C}^{*(2)}\right)\left(\Psi_{i+1/2}(s)\right)\left(\frac{d\psi_{i+1/2}^{(1)}}{ds},....,\frac{d\psi_{i+1/2}^{(N)}}{ds}\right)^T ds\end{aligned} \tag{12}$$

$B_1^{*(4)}$ is the fourth non-zero entry (namely u_b) of the vector B_1^*. We note this term by

$$\left(B_1^{*(4)}\right)_{i+1/2}^{\Psi} = u_b^* \quad (13)$$

u_b^* does not depend on unknown variables. Using the linear path, a very accurate numerical approximation of the characteristic velocity of body sedimentary also can be given by

$$u_b^* = \int_0^1 u_b(s)ds = \sum_{g=1}^{NGp} w_g u_b(s_g), \tag{14}$$

where NGp is several points Gauss quadrature rule, w_g are the weights and s_g are the positions distributed in the unit interval $[0,1]$. As an example, using a three-point Gaussian quadrature rule with the following points s_g and

$$s_1 = \frac{1}{2},\ s_{2,3} = \frac{1}{2}\pm\frac{\sqrt{15}}{10},\ w_1 = \frac{8}{18},\ w_{2,3} = \frac{8}{15}, \tag{15}$$

In all the numerical simulations, one point-Gauss quadrature is used and therefore we have:

$$u_b^* = w_1 u_b(s_1) \tag{16}$$

This choice allows us to ensure the achievement of the second accuracy in
space. Here, a piecewise polynomial reconstruction is applied W, that is:

$$\begin{aligned}W(x) &= \sum_i \mathbf{P}_i(x)\chi_{K_i}(x),\\ \mathbf{P}_i &= \left(P_i^{(1)},P_i^{(2)},...,P_i^{(N)}\right)^T\end{aligned} \tag{17}$$

The local speeds velocities using Eq.(6) are given by:

$$\begin{aligned}a_{i+1/2}^{+} &= \max\left\{u_{i+1/2}^{-}+\sqrt{gh_{i+1/2}^{-}},u_{i+1/2}^{+}+\sqrt{gh_{i+1/2}^{+}},0\right\}\\ a_{i+1/2}^{-} &= \min\left\{u_{i+1/2}^{-}-\sqrt{gh_{i+1/2}^{-}},u_{i+1/2}^{+}-\sqrt{gh_{i+1/2}^{+}},0\right\}\end{aligned} \tag{18}$$

Note that at the first-order, we have:

$$\begin{aligned}W_{i+1/2}^{+} &= \mathbf{P}_i(x_{i+1/2}) = \overline{W}_{i+1}\\ W_{i+1/2}^{-} &= \mathbf{P}_{i+1}(x_{i+1/2}) = \overline{W}_i\end{aligned} \tag{19}$$

The CFL condition reads:

$$\Delta t \le CFL \frac{\Delta x}{2\max(a^+_{i+1/2}, -a^-_{i+1/2})};\ \ 0 < CFL \le 1 \quad (20)$$

where Δt is the step time?

$$\left(B_1^*\right)_i = \left(0;\ \frac{g}{2}\left(h^-_{i+1/2} + h^+_{i-1/2}\right)\left(\Delta Z_b\right);\ u_b^*\left(\Delta Z_b\right)\right)^T \quad (21)$$

$$B^*_{2,i} = (0, A_1, 0, 0)^T,$$

$$A_1 = -\frac{\delta\rho}{2\rho} g\left[\left(h^-_{i+1/2} + h^+_{i-1/2}\right)\Delta(hC) - \left((hC)^-_{i+1/2} + (hC)^+_{i+1/2}\right)\Delta(h)\right] \quad (22)$$

Using the definition of the linear path, we have:

$$\left(B_1^{*(2)}\right)^{\Psi}_{i+1/2} = \frac{g}{2}\left(h^-_{i+1/2} + h^+_{i+1/2}\right)\left(Z^+_{b,i+1/2} - Z^-_{b,i+1/2}\right) \quad (23)$$

$$\left(B_2^{*(2)}\right)^{\Psi}_{i+1/2} = -\frac{(\rho_s - \rho_w) g}{2\overline{\rho}_i}\left[\left(h^-_{i+1/2} + h^+_{i+1/2}\right)\Delta(hC) - \left((hC)^-_{i+1/2} + (hC)^+_{i+1/2}\right)\Delta(h)\right] \quad (24)$$

Remark. The first-order semi-discrete scheme is given by Eqs.(9)-(13), (16)-(19) PCCU and (22)-(24). It's necessary to improve the numerical solution of the proposed first-order scheme by processing the solution on the edges of each cell. This leads to achieving the second order in space. For this reason, we use a new AENO reconstruction technique.

4 Second Order WBPP Semi-Discrete PCCU Scheme

In this section, we develop a second-order PCCU semi-discrete scheme to improve the solution. We prove that the proposed is well-balanced and preserves the positivity of the water depth. We use first, a modified AENO reconstruction procedure of Toro *et al*, [36], and second, we develop a strategy to maintain the balance between the flux and source terms.

4.1 AENO Reconstruction

In the above first-order semi-discrete scheme, the piecewise polynomial given by Eq. (17) is assumed constant. To deal with the second-order scheme, we adopt the new expression for the reconstruction W given by W expressed as:

We have chosen in this scheme the simplest linear segment path given by:

$$\Psi_{i+1/2}(s) = W^-_{i+1/2} + s(W^+_{i+1/2} - W^-_{i+1/2}),\ s \in [0,1] \quad (21)$$

Using this path, the discrete nonconservative terms read:

$$W(x) = \sum_i \mathbf{P}_i(x)\chi_{K_i}(x),\ \ \mathbf{P}_i = \left(P_i^{(1)}, P_i^{(2)}, ..., P_i^{(N)}\right)^T$$

where $\mathbf{P}_i(x)$ is given by:

$$\mathbf{P}_i(x) = \bar{W}_i + \Delta_i(x - x_i);\ x \in K_i, \quad \text{with } x_i = \frac{x_{i+1/2} - x_{i-1/2}}{2}, \quad (25)$$

where $\Delta_i = (\nabla W)_i$ are the slopes that approximate $(\nabla W(x_i, t^n)$ in a non-oscillatory manner using a nonlinear slope obtained by a convex combination of $\Delta_{i+1/2}$ *and* $\Delta_{i-1/2}$ as follows

$$(\nabla W^n)_i = \Delta^n{}_i = \beta\Delta^n_{i+1/2} + (1-\beta)\Delta^n_{i-1/2},\ \ \beta \in [0,1] \quad (26)$$

where $\beta(r) = \frac{r}{\sqrt{l^2 + r^2}}$; with $r = \frac{\Delta_{i-1/2}}{\Delta_{i+1/2} + \varsigma}$ and where $\Delta_{i+1/2} = \frac{\bar{W}_{i+1} - \bar{W}_i}{\Delta x}$, $\Delta_{i-1/2} = \frac{\bar{W}_i - \bar{W}_{i-1}}{\Delta x}$ l is a positive parameter, ς is a small positive tolerance to avoid division by zeros. The resulting semi-discrete second-order PCCU-AENO scheme (given by equations (9)-(13), (22)-(24), and (25)-(26)) is then obtained by using the new expression W in all the above equations. Next, for the sake of simplicity, we take W instead of W .

4.2 Well-balanced Strategy of the Scheme

The well-balanced property of our scheme is obtained when the discrete version of the source terms $\overline{S}_{0,i}, \overline{S}_{c,i}, \overline{S}_{e,i}, \overline{S}_{F,i}$ exactly balances the numerical fluxes so that the right-hand-side (RHS) of Eq. (9) vanishes for 'lake at rest' steady states $W = \left(h_0, 0, K_0, b_0\right)$, where $h_0, 0, K_0, b_0$, are the non-negative constants. In this subsection, we present an approach to achieve a well-balanced path-conservative central-upwind method, by an existing approach recently developed by Ngatcha *et al*, [14].

For these steady states $W^+_{i+1/2} = W^-_{i+1/2}\ \ \forall i$. Moreover, the C-property is satisfied if the condition:

$$E - D = 0,\ hC = K_0,\ h = h_0,\ u = 0,\ Z_b = b_0, \rho = C_0 \quad (27)$$

where K_0, h_0, b_0, C_0 are nonnegative constants (valid for stationary flows at rest) is verified. For the stationary solutions, we have $\frac{d\overline{W_i}}{dt}=0$. And according to Eq. (9), we have:

$$\begin{aligned}
&\mathrm{F}^{(1)}_{i+1/2}-\mathrm{F}^{(1)}_{i-1/2}+S^{(1)}_{e,i}=0,\\
&\mathrm{F}^{(2)}_{i+1/2}-\mathrm{F}^{(2)}_{i-1/2}-B^{*(2)}_{1,i}-B^{*(2)}_{2,i}+\mathrm{H}^{(2)}_{i+1/2}-\mathrm{H}^{(2)}_{i-1/2}=0,\\
&\mathrm{F}^{(3)}_{i+1/2}-\mathrm{F}^{(3)}_{i-1/2}+S^{(3)}_{e,i}=0,\\
&\mathrm{F}^{(4)}_{i+1/2}-\mathrm{F}^{(4)}_{i-1/2}+S^{(4)}_{e,i}=0.
\end{aligned} \tag{28}$$

Therefore, we have the following well-balanced discretization for the topography source term:

$$B^{*(2)}_{1,i}+B^{*(2)}_{2,i}=\mathrm{F}^{(2)}_{i+1/2}-\mathrm{F}^{(2)}_{i-1/2}+\mathrm{H}^{(2)}_{i+1/2}-\mathrm{H}^{(2)}_{i-1/2} \tag{29}$$

Here, the numerical flux according to Equation (21) reads:

$$\mathrm{F}^{(2)}_{i+1/2}=\frac{a^{+}_{i+1/2}}{a^{+}_{i+1/2}-a^{-}_{i+1/2}}(0.5g(h^{-}_{i+1/2})^2)-\frac{a^{-}_{i+1/2}}{a^{+}_{i+1/2}-a^{-}_{i+1/2}}(0.5g(h^{+}_{i+1/2})^2)$$

The nonconservative contribution reads:

$$\mathrm{H}^{(2)}_{i+1/2}=\frac{a^{-}_{i+1/2}}{a^{+}_{i+1/2}-a^{-}_{i+1/2}}\left(\left(B^{*(2)}_{2}\right)^{\Psi}_{i+1/2}+\left(B^{*(2)}_{1}\right)^{\Psi}_{i+1/2}\right) \tag{30a}$$

where using the fact that

$\eta^{+}_{i+1/2}=h^{+}_{i+1/2}+Z^{+}_{b,i+1/2}$, $\eta^{-}_{i+1/2}=h^{-}_{i+1/2}+Z^{-}_{b,i+1/2}$,

we obtain the following well-balanced discretization of topography nonconservative term

$$\left(B^{*(2)}_{1}\right)^{\Psi}_{i+1/2}=-g\frac{\left(h^{+}_{i+1/2}+h^{-}_{i+1/2}\right)}{2}\left(h^{+}_{i+1/2}-h^{-}_{i+1/2}\right). \tag{30b}$$

Here, the reconstruction values of unknowns are given by using the AENO reconstruction procedure. The well-balanced discretization PCCU scheme is finally obtained by replacing $B^{*(2)}_{1,i}$ given by (23) in the semi-discrete scheme (9) $B^{*(2)}_{1,i}$ given by Eq. (30b). With this discretization procedure, the proposed scheme is well balanced. The first, third, and last equations are trivial. The discrete source terms S_e, S_F and S_D read:

$$S_{e,i}=\begin{pmatrix}\frac{E-D}{1-p}\\ -\frac{(E-D)u_i}{(1-p)}\\ E-D\\ -\frac{E-D}{1-p}\end{pmatrix},\ S_{F,i}=\begin{pmatrix}0\\ -g\frac{\left(h^{-}_{i+1/2}+h^{+}_{i-1/2}\right)}{2}S_{f,i}\\ 0\\ 0\end{pmatrix},$$

$$S_{D,i}=\begin{pmatrix}0\\ 0\\ \left(\nu_m\left(f_{s,i+1/2}h^{-}_{i+1/2}\frac{C_{i+1}-C_i}{dx}-f_{s,i-1/2}h^{+}_{i-1/2}\frac{C_i-C_{i-1}}{dx}\right)\right)\\ 0\end{pmatrix} \tag{31}$$

Here, we have used the central scheme to discretize the diffusion source term. The semi-discrete PCCU-AENO scheme above given by equations (9)-(13), (22)-(24), and (25)-(26) with the equations (30)-(31) satisfies the C-property.

4.3 AENO Preserving-positivity Procedure

Here, we propose a procedure called AENO-preserving positivity reconstruction to achieve both the positivity of water depth and the C-property of the scheme. We use the reconstructed values of the unknowns to the left and right of $i+1/2$ the AENO technique developed above $h^{\pm}_{i+1/2}, q^{\pm}_{i+1/2}, Z^{\pm}_{b,i+1/2}$. The left/right velocities and concentrations are calculated as:

$$\begin{aligned}
u^{+}_{i+1/2}&=\frac{(hu)^{+}_{i+1/2}}{h^{+}_{i+1/2}},\quad u^{-}_{i+1/2}=\frac{(hu)^{-}_{i+1/2}}{h^{-}_{i+1/2}}\\
C^{+}_{i+1/2}&=\frac{(hC)^{+}_{i+1/2}}{h^{+}_{i+1/2}},\quad C^{-}_{i+1/2}=\frac{(hC)^{-}_{i+1/2}}{h^{-}_{i+1/2}}
\end{aligned} \tag{32}$$

The bottom reconstruction at left and right is given by:

$$\begin{aligned}
\overline{Z}^{+}_{b,i+1/2}&=\min\left(\max\left(\overline{Z}_{b,i},\overline{Z}_{b,i+1}\right),\overline{\eta}_{i+1}\right),\\
\overline{Z}^{-}_{b,i+1/2}&=\min\left(\max\left(\overline{Z}_{b,i},\overline{Z}_{b,i+1}\right),\overline{\eta}_{i}\right),
\end{aligned} \tag{33}$$

and the discrete free surface is

$$\overline{\eta}_{i+1} = \overline{h}_{i+1} + \overline{Z}_{b,i+1},\ \overline{\eta}_i = \overline{h}_i + \overline{Z}_i \tag{34}$$

Which verified at the steady states:

$$\overline{h}^{*,-}_{i+1/2} = \overline{h}^{*,+}_{i+1/2},\quad \overline{h}^{-}_{i+1/2} = \overline{h}^{+}_{i+1/2}, \tag{35}$$

where

$$\overline{h}^{*,-}_{i+1/2} = \min\left(\overline{\eta}_i - \max\left(\overline{Z}^{-}_{b,i+1/2}, \overline{Z}^{+}_{b,i+1/2}\right), \overline{h}_i\right),$$

$$\overline{h}^{*,+}_{i+1/2} = \min\left(\overline{\eta}_{i+1} - \max\left(\overline{Z}^{-}_{b,i+1/2}, \overline{Z}^{+}_{b,i+1/2}\right), \overline{h}_{i+1}\right)$$

The preserving-positivity procedure of water, depth is given by:

$$h^{\pm}_{i+1/2} = \max\left(0,\ h^{*,\pm}_{i+1/2}\right) \tag{36}$$

The water discharge and the sediment flux are respectively:

$$\overline{q}^{\pm}_{i+1/2} = \overline{h}^{\pm}_{i+1/2}\overline{u}^{\pm}_{i+1/2},\ \left(\overline{hC}\right)^{\pm}_{i+1/2} = \overline{h}^{\pm}_{i+1/2}\overline{C}^{\pm}_{i+1/2} \tag{37}$$

Remark. The fully discrete PCCU scheme.
The fully discrete PCCU scheme is obtained by using a variant of the strong stability preserving (SSP) method also called the third-order semi-implicit Runge-Kutta (SI-RK3) method originally developed by Chertock *et al*, [37], for the shallow water equations and recently applied for Saint-Venant-Exner equations by Ngatcha *et al*, [14]. The discrete PCCU scheme is also well-balanced and preserves the positivity of the water depth.

Remark. The semi-discrete PCCU-AENO scheme above given by equations (9)-(13), (22)-(24), and (25)-(26) with the equations (30)-(37) satisfies the C-property and preserves the positivity of the water depth.

5 Results and Discussion

The computational parameters are given in Table 1 and the AENO reconstruction is performed with ς = 0.0001 and $l = 1$. The Neumann condition is adopted here.

Table 1. Parameters used for the simulation

Parameters	Values
ρ_w	$1000\ Kg/m^3$
ρ_s	$2650\ Kg/m^3$
φ	$0.015\,m^{1.2}$
ν	$1.2\times10^{-6}\,m^2/s$
p	0.4
g	9.81
n	0.028
d_{50}	0.001

5.1 Accuracy test. SWE

To check the accuracy of the proposed method, we consider the SWE, [11]. Here, the sediment transport is removed. i.e., $C(x,t) = 0$ $E - D = 0$ $u_b = 0$ the domain of simulation is the channel of length $L = 2000m$. The initial conditions are given:

$$h(x,0) = \begin{cases} 10 & \text{if } x \le 1000m \\ 5 & \text{if } x > 1000m \end{cases},\quad u(x,0) = 0. \tag{38}$$

We use zero-order extrapolation at all of the boundaries. The solution obtained by our scheme at the final time $t = 30s$ is compared with the exact solution. The comparison tests of the velocity and water depth are plotted and illustrated in Fig. 4.

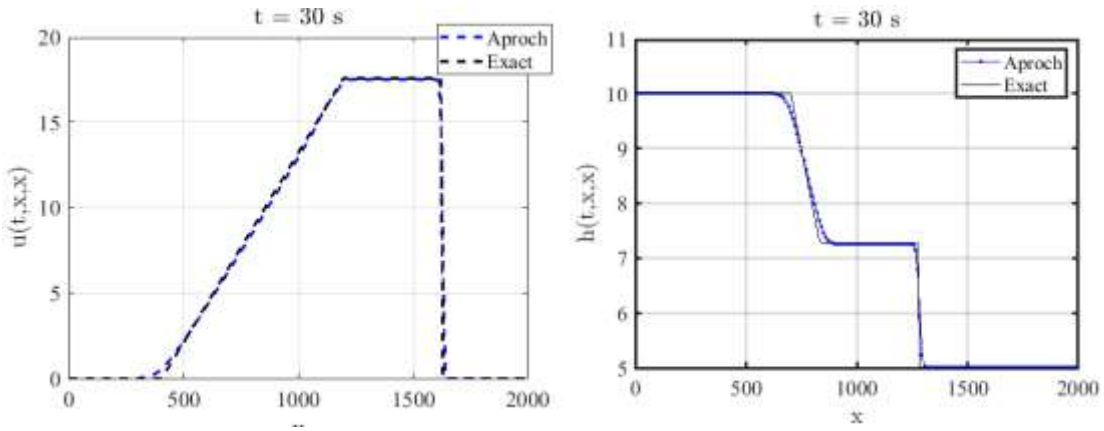

Fig. 4: Comparison between the exact solution and numerical solution at the first order

The result presented in Fig. 4 shows that the shocks are well captured during the simulation. The calculated numerical solution agrees very well with the exact solution. The profiles of water height and velocity are well represented and the physical properties of the studied problem are preserved.

5.2 Verification of C-property

Here, we validate the *C*-property of the PCCU scheme in the context of the full sediment transport equations. For this purpose, a slightly modified version of the test case proposed by, [17], is solved in the following. The initial conditions read:

$$h(x,0)=0.2,\ \ Z_b(x,0)=0.1+0.1\exp((-x-5)^2),$$
$$\mathrm{u}(x,0)=0 \text{ and } \mathrm{C}(x,0)=0. \tag{39}$$

The rest of the computational parameters are available in Table 1. The final computational times are $t=0,\ t=0.05,\ t=5$. The calibration parameter is $C_s=0.8$. The computational grid is composed of 400 cells and the CFL number has been set to 0.9. We solve this problem without any perturbation of the
free surface to verify the exact well-balance of our scheme. For all these three cases, the steady states should be exactly preserved. The results are plotted and exposed in Fig. 5.

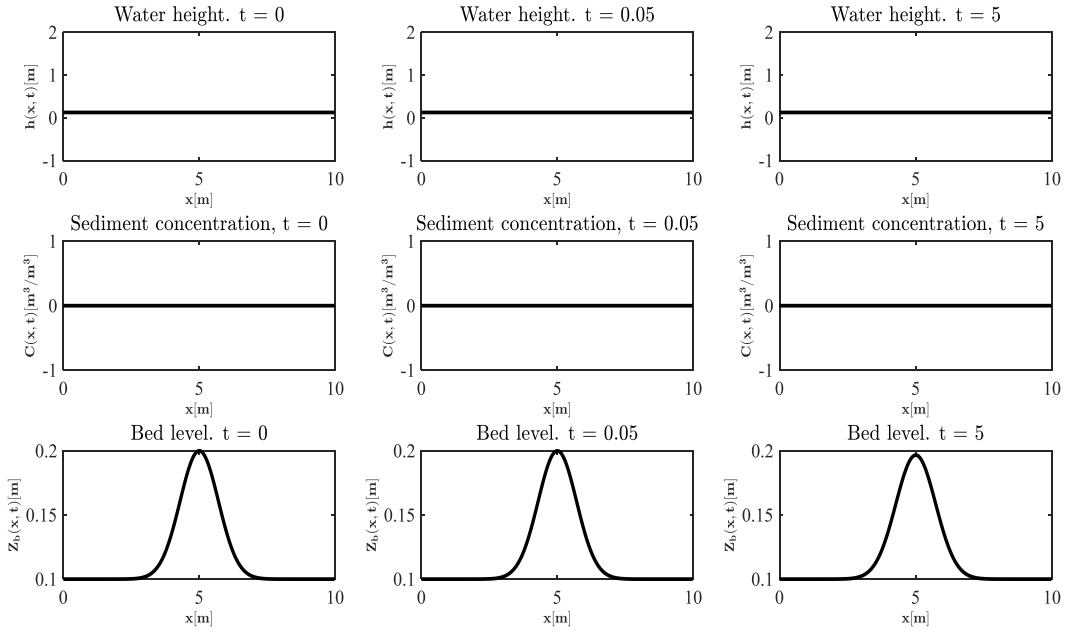

Fig. 5: Well-balanced test with different time simulations.

It is expected that the free surface remains constant and the sediment concentration should be zero at all times. We can observe that there are no spurious numerical oscillations and the propagated small perturbation is very well captured by the proposed well-balanced methods. This small perturbation erodes the sediment bed and decreases very weakly its height $\overline{Z}_{b,i}^{n} \approx Z(x,0)$. This phenomenon is well observed in nature. Therefore, the proposed well-balanced PCCU-AENO method preserves the C-property to the machine's precision.

5.2 Dam Break over the Erodible Bed without Sediment Diffusion. Influence of Calibration Parameter C_s

We recall that dam breaks are characterized by a sudden fall of water initially placed at a certain height on a moving floor and cause
strong variations of fluid and sediment velocities. The main objective is to assess the performance of the PCCU scheme described above to compute the dam break problem. A similar test is also done in, [21] (see also, [23]). We consider the rectangular channel of length $L=1m$ with a dam located in the middle of the domain. The initial conditions are given:

$$h(x,0)=\begin{cases}2 & \text{if } x\le 0.5\\ 0.125 & \text{if } x>0.5\end{cases},\ u(0,x)=0,\quad (40)$$
$$Z_b(0,x)=0,\ C(x,0)=0,$$

and zero-order extrapolation is used at all of the boundaries.

Here, we have assumed that $u_b(Z_b)\dfrac{\partial Z_b}{\partial x}=0$. We find a hyperbolic system similar to that developed by Cao *et al*, [23], and solved by using flux-limited methods, [21]. The eigenstructure of the system is well-known and is available in, [21]. In this situation, the resonance phenomenon disappears and all the characteristic fields are not completely degenerated. The computational parameters are given in Table 1. The numerical solution for this test computed using the proposed scheme is shown in Fig. 6

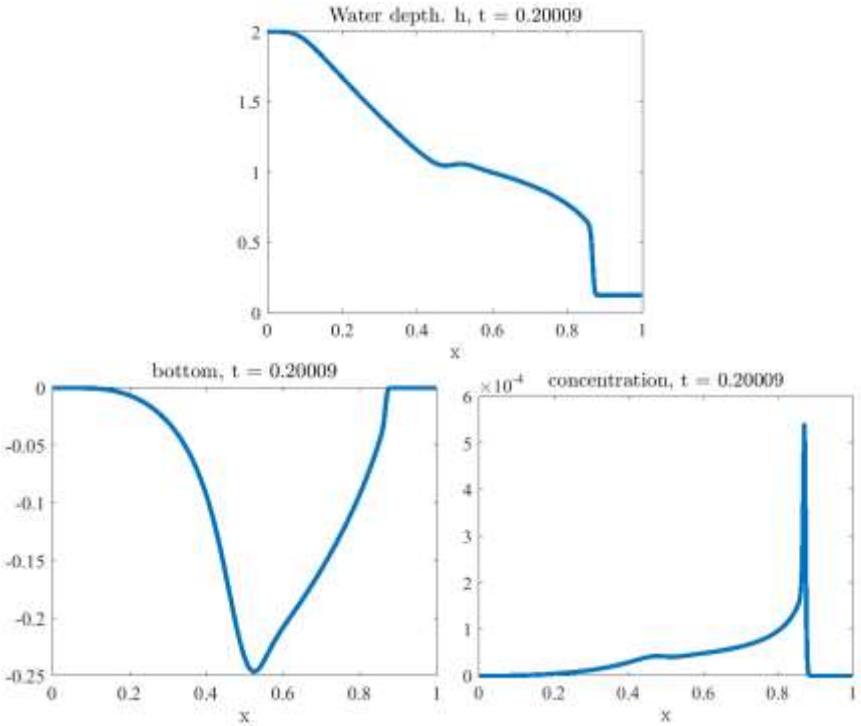

Fig. 6: Water depth, sediment concentration, bed level, and velocity profiles with PCCU-AENO, we have used N=200 cells grid, CFL = 0.1.

It is expected that the bed level profile in Fig. 6 is similar to that obtained in, [21], by using the Flux limiter method and by experiment data in [24].
Now we consider the movement of the bed with characteristic velocity u_b i.e. $u_b(Z_b)\dfrac{\partial Z_b}{\partial x}\neq 0$ ..... We use the same computational parameters as the previous test. The time of simulation is $t=0.2$. The computational solution is plotted in Fig. 7.

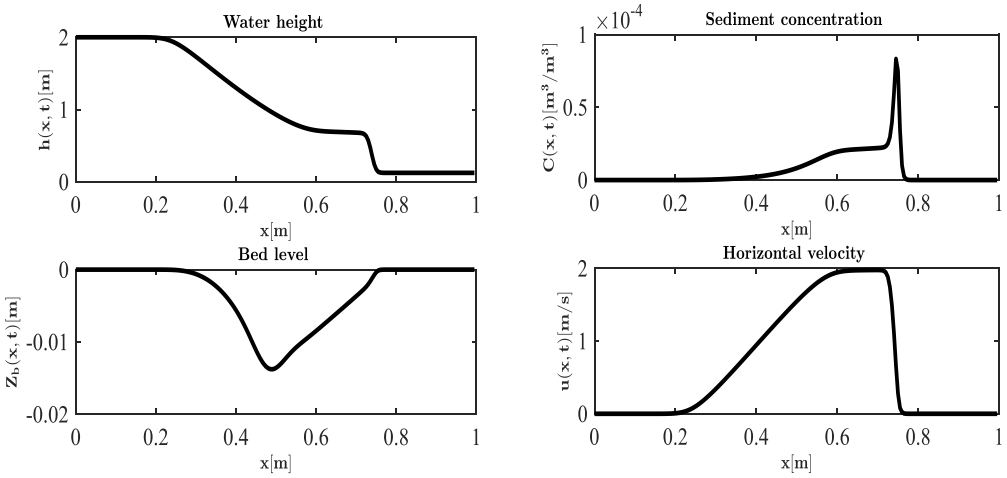

Fig.7: Water height, sediment concentration, bed level, and velocity profiles with PCCU-AENO, we have used N=200 cells grid, CFL = 0.1. The calibration parameter is $C_s = 0.45$

As one can see in Fig. 7, even under a high-energetic flow considered in this example, the fully coupled model can predict a stable bed erosion process and leads to a smooth and physically expectable bed profile.

Now we compare both the PCCU-AENO scheme and the CU-AENO scheme when the sediment diameter is $d = 0.0001$. The results of both schemes at different times are plotted in Fig. 8. It is expected that the model can be solved by a CU scheme dealing with the non-conservative terms as source terms that physically is not clear. At the time $t = 0.1$, the CU scheme does not capture the shock well. We can observe that there are no spurious numerical oscillations and the propagated fluid after the break is very well captured by the proposed well-balanced methods.

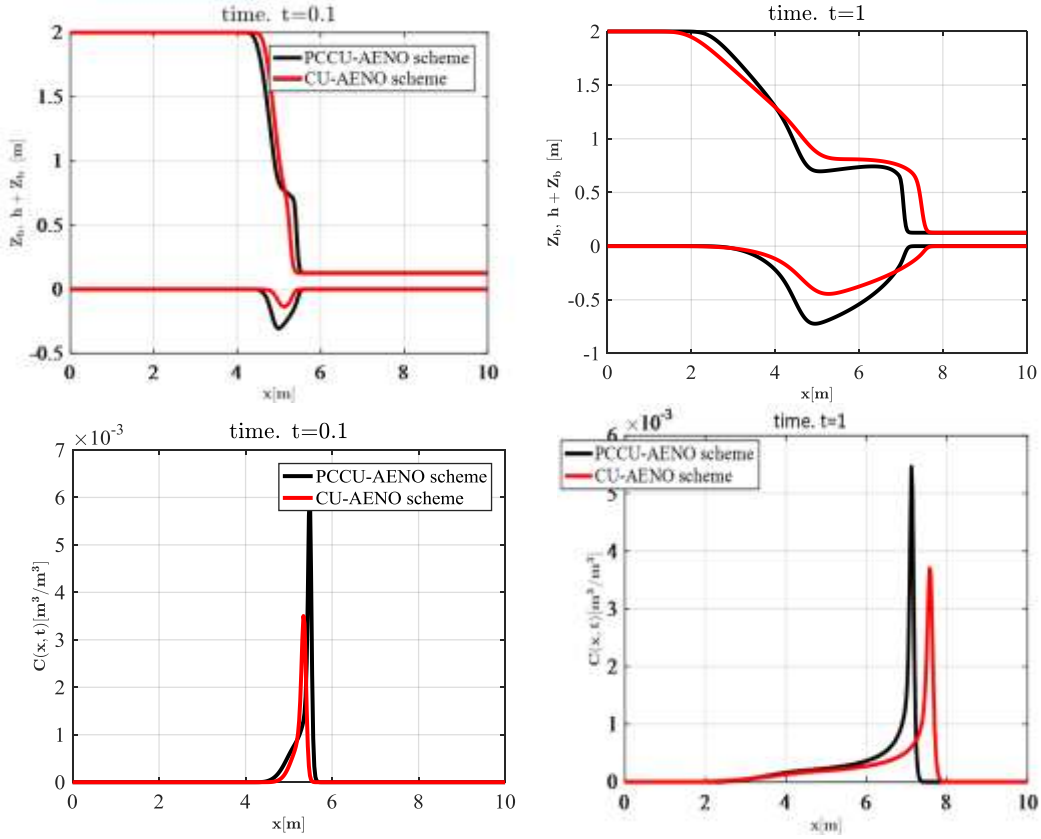

Fig. 8: Comparison between the CU-AENO scheme and PCCU-AENO scheme for an erodible dam-break problem.

The computational parameters are CFL = 0.5, N= 200 grid cells, $C_s = 0.5$ A variant of this test is given by the following initial conditions:

$$h(x,0) = \begin{cases} 2 & \text{if } x \le 0.5 \\ 0 & \text{if } x > 0.5 \end{cases}, \; u(x,0) = 0, \qquad (41)$$
$$Z_b(x,0) = 0.1 + 0.1\exp((-x-5)^2), \; C(x,0) = 0.$$

We compare again both PCCU schemes for two classes of size grains to see the advantage of our method. The results obtained by our model are plotted in Fig. 9. We expect that the proposed model can apply to a large range of sediment sizes. Therefore, it can be applied in several environments

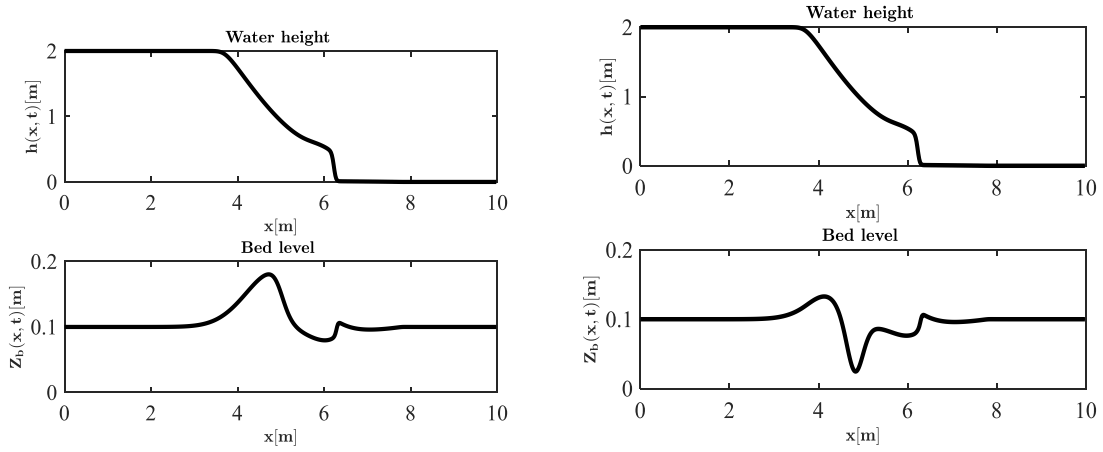

Fig. 9: Dam break over erodible sediment bum. Left, first-order PCCU scheme with C_s =0.75, right first-order PCCU scheme with C_s =0.25. The computational parameters are $t = 0.5$ N=200 uniform grid cells, CFL = 0.1.

It is expected that the first-order PCCU method has been successful in eliminating the numerical diffusion, and it does not give rise to nonphysical oscillations near regions of large gradients. The non-entropic character is not observed in the rarefaction wave zone. The test proves that our scheme can deal a sediment transport even in presence of a dry zone and for a large range of characteristic velocities u_b (that depends on sediment size).

5.3 Dam-break over Erodible Bed: Comparison between the Proposed Model (M1), SVE Model through Grass Formula (M2), and Experiment Data

In this test, the SVE model with the Grass formula is solved and compared to the proposed sediment transport model and experiment data. A similar test is done by Gunawan, Fraccarrolo, and Capart, [24]. SVE model is obtained when $E - D = 0$ and when we remove the sediment concentration equation. The initial conditions read:

$$h(x,0) = \begin{cases} 0.1 & \text{if } x \le 0 \\ 0 & \text{if } x > 0 \end{cases}, \; u(0,x) = 0, \qquad (42)$$
$$Z_b(0,x) = 0.$$

For the classical Exner model, the sediment diameter is $d_{50} = 0.0032$, sediment density is $\rho_s = 1.540$, and the domain of simulation is $\Omega = [-1.25; 1.25]$. Grass formula is used with $A_g = 0.005$, $m = 3$. Free surface and bed level profiles at a time $t = 0.5$, $t = 0.75$ and $t = 1$ is computed and shown in Fig. 10. They show a good agreement between the numerical computation and the experimental data of, [24], concerning the water level and bed sediment profiles. The difference between both models is plotted in Fig. 11.

The results obtained by the PCCU scheme show that the proposed model converges better with the experimental data of Fraccarolo and Capart [24] than the classical model. We have used it in all the simulations $CFL = 0.1$, $N = 100$ and cells. We observe that the water level and sediment bed profiles are better approximated using the PCCU scheme. The profile of the bed level is obtained by the appropriate choice of calibration parameter C_s. This shows the importance of the characterization of sediment velocity u_s

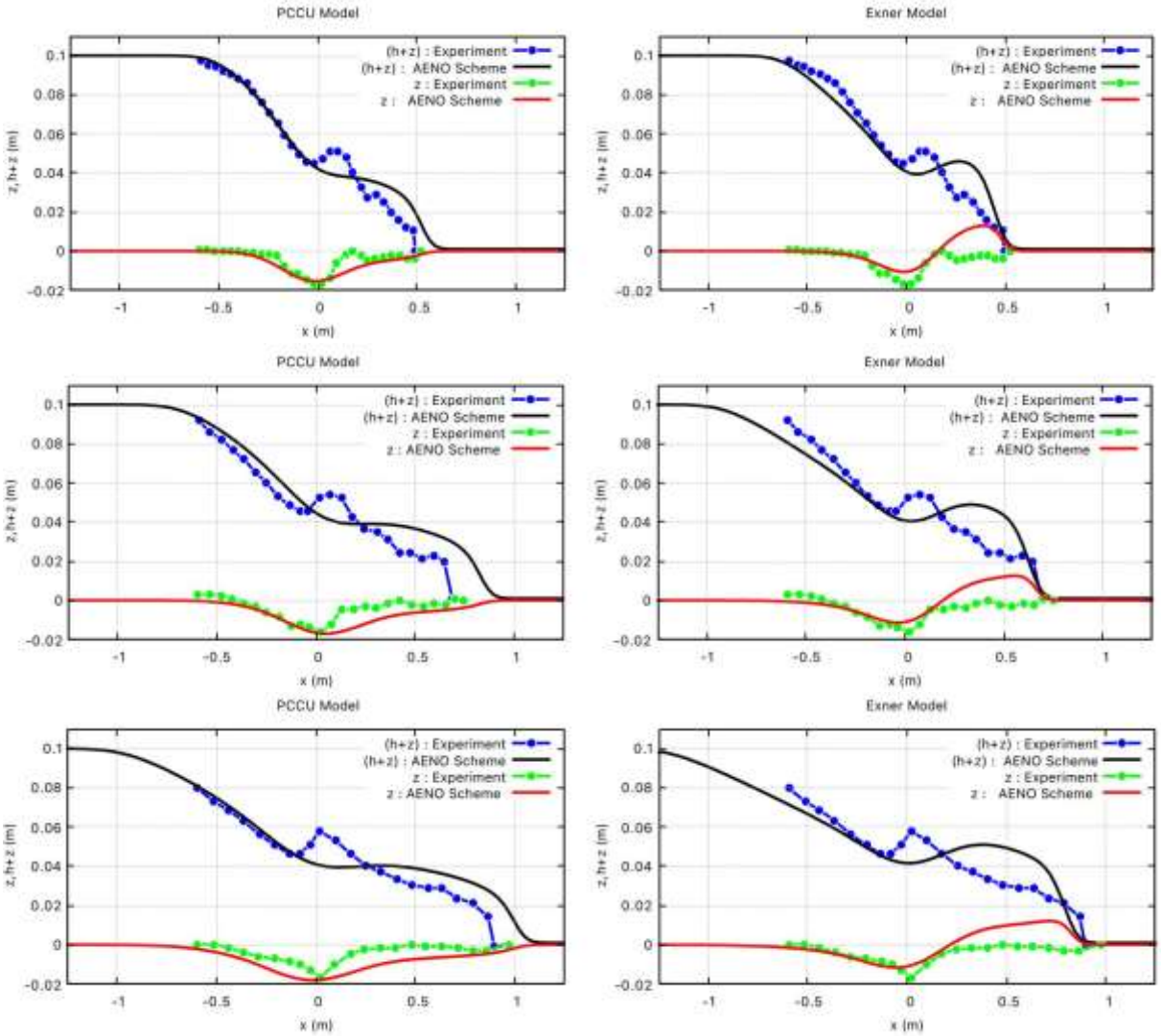

Fig. 10: Comparison between the proposed model solved using the PCCU-AENO scheme (PCCU model), Saint-Venant-Exner model (Exner model), and the experiment data. The different simulation times from top to bottom are t=0.5s, t=0.75s, and t=1s respectively. Here, $z = Z_b$

We can see that the classical SVE does not capture the bed evolution very well during the different times.

The results presented in Fig. 10, using the Exner model, are very similar to those reported in, [25], using the finite volume staggered grid. A clear observation is that the study of morphodynamics with an SVE model is not realistic.

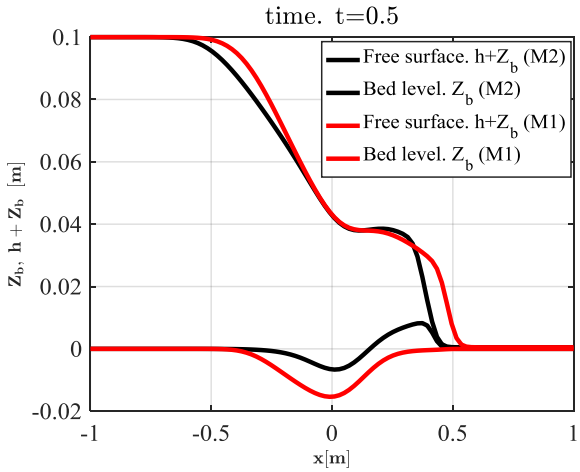

Fig. 11: Numerical solution $h + Z_b, Z_b$.

Comparison between the proposed model (M1) and the classical model (M2) at time t=0.5. For the proposed model, we have taken $C_s = 0.55$.

We observe that in both cases, as time progresses, the flow adopts a rather sharp profile at the wavefront, consistent with the physics of shallow-water flows.
Therefore, from the Figs. (10)-(11), we have proven that the classical Exner model cannot accurately describe the movement of a sand wave on the bottom, and can't let us know the speed at which the bottom is moving.

6 Conclusion and Perspectives

This paper has presented a novel sediment transport model based on shallow water equations. We have proposed for this model a new bed-load equation. This new equation has the particularity of integrating the phase lag effect and can help to know the characteristic velocity with which the bottom moves. With this new equation, the fully coupled model resulting is hyperbolic and admits a simple eigenstructure. This eigenstructure can be determined without the use of the Lagrange or Gerschgorin theorems. A second-order path-conservative central-upwind scheme has been proposed for solving the proposed sediment transport model. The fluctuations at left/right are easily computed. The second order of accuracy is achieved by using a nonlinear reconstruction technique called AENO. A strategy of well-balanced discretization has been implemented here. Moreover, AENO hydrostatic reconstruction also has been proposed to maintain the positivity of the scheme. The resulting scheme has been proven well-balanced and preserving-positivity. SI-RK3 time discretization allowed us to obtain a second-order accuracy in time. Several numerical tests are made to assess the accuracy, convergence, well-balancedness, and positivity of the water depth and performances of the proposed shock-capturing method. The proposed model gives good and realistic results. The proposed one-dimensional numerical methods can solve several arbitrary hyperbolic systems, both in conservative and nonconservative forms. The proposed scheme can simulate flooding with sediment deposition in a section of the TONGO BASSA basin located in Douala Cameroon (this is future research).

Acknowledgment
The authors would like to thank an anonymous referee for giving very helpful comments and suggestions that have greatly improved this paper.

References:

[1] G. Cannata, L. Barsi et M. Tamburrino, «A 3D numerical model for turbudity currents,» *WSEAS TRANSACTIONS on FLUID MECHANICS,* vol. 15, n° %11, 2020.

[2] A. H. N. Chegini et G. Pender, «Determination of small size bedload sediment transport and its related bedfrom under uniform flow conditions,» *WSEAS TRANSACTIONS on ENVIRONMENT and DEVELOPMENT,* vol. 8, n° %14, pp. 158-167, 2012.

[3] F. Exner, «Uber die Wechselwirkung zwischen Wasser und Geschiebe in Flussen.,» *Akademie der Wissenschaften,* vol. Sitzungsberichte 134, 1925.

[4] B. Greimann et J. Huang, «Two-dimensional total sediment load model equations.,» *Haudraul Eng,* vol. 134, pp. 1142-1146, 2008.

[5] P. Tassi et C. Villaret, Sisyphe v6.3 User's Manual. EDF R&D., Chatou, France, 2014.

[6] M. VAH, A. JARNO, F. MARIN et S. LE BOT, «Experimental Study on Sediment Supply-Limited Bedforms in a Coastal Context,» chez *Sixth International Conference on Estuaries and Coasts (ICEC-2018)*, Caen, France, August 20-23, 2018.

[7] R. C. van, «Sediment Transport, Part II: Suspended Load Transport.,» *Journal of Hydraulic Engineering* , vol. 110, p. 1613—1641, 1984.

[8] L. Van Rijn, R. Bisschop et C. Van Rhee, «Modified sediment pick-up function,» *Journal of Hydraulic Engineering,* vol. 145, p. p.~06018017, 2019.

[9] Soulsby, Dynamics of marine sands, a manual for practical applications, Vols. %1 sur %2ISBN 0-7277-2584X, Wallingford: Thomas Telford, 1997.

[10] A. J. Grass, «Sediment transport by waves and currents,» Department of civil engineering, University college , London, 1981.

[11] B. d. A. Saint-Venant, «Théorie du mouvement non-permanent des eaux avec application aux crues des rivières et à

l'introduction des marées dans leur lit,» *Comptes Rendus de L'Académie des sciences,* vol. 73, pp. 147-154, 1871.

[12] F. Gallerano, M. L et G. Cannata, «The dynamic procedure for closure relations in the equation of the filtered concentration of ssupended solids particles,» *WSEAS TRANSACTIONS ON FLUID MECHANICS ,* vol. 1, n° %1ISSN 1790-5087, pp. 738-744, 2006.

[13] E. Alqasimi, K. Tew et K. Mahdi, «A new one-dimensional numerical model unsteady hydraulic of sediments in rivers,» *SN APPLIED SCIENCES ,* vol. 2, n° %11480, 2020.

[14] A. Ngatcha et A. Njifenjou, «A well balanced PCCU AENO scheme for a sediment transport model,» *Ocean System Engineering,* vol. 12, n° %13, pp. 359-384, 2022.

[15] I. Moungnutu, A. Ngtacha et A. Njifenjou, «Stabilization of a finite solution for 1D Shallow Water problems,» *Preprint ResearchGate,* 2022.

[16] C. Giovanni, F. Lapsaponara et F. Gallerano, «Non-Linear Shallow Water Equations Numerical integration on curvilinear boundary-Conforming grids,» *WSEAS TRANSACTIONS on FLUID MECHANICS,* vol. 10, pp. 13-25, 2015.

[17] L. Xin, M. Abdolmajid, K. Alexander et A. I. S. Julio, «Well-balanced central-upwind scheme for a fully coupled shallow water system modeling flows over erodible bed,» *Journal of Computational Physics,* vol. 300 , p. 202–218, 2015.

[18] A. R. Ngatcha, B. Nkonga et A. Njifenjou, «Multi-dimensional Positivity-preserving Well-balanced Path-Conservative Central-Upwind scheme on unstructured meshes for a total sediment transport model,» *https://hal.archives-ouvertes.fr/hal-03668107.,* 2022.

[19] A. Siviglia, D. Vanzob et E. Toro, «A splitting scheme for the coupled Saint-Venant-Exner model,» *Advances in Water Resources,* vol. 159, p. 104062, 2022.

[20] A. Ngatcha et A. N. B. Njifenjou, «Finite volume AENO methods with flux time-steps discretization procedure for a averaged sediment transport model,» *https://hal.archives-ouvertes.fr/hal-03668098,* 2022.

[21] F. Benkhaldoun, S. Saida et M. Seaid, «A flux-limiter method for dam-break flows over erodible sediment beds,» *Applied Mathematical Modelling,* vol. 36, n° %12012, p. 4847–4861, 2012.

[22] Z. Cao, R. Day et S. ,. Egashira, «Coupled and uncoupled numerical modelling of flow and morphological evolution in alluvial rivers,» *Journal of Hydraulic Engineering,* vol. 128, n° %13, pp. 306-321, 2002.

[23] Z. Cao, G. Pender, S. Wallis et P. Carling, «Computational dam-break hydraulics over erodible sediment bed,» *Journal Hydraulic Engineering,* vol. 130(7), pp. 689-703, 2004.

[24] L. Fraccarollo et H. Capart, «Riemann wave description of erosional dam-break flows,» *J. Fluid Mech.,* vol. 461, pp. 183-228, 2002.

[25] P. H. Gunavan, «Numerical simulation of shallow water equations and related models,» Phd Thesis, Université de Paris-Est, HAL Id: tel 01216642, Paris-Est.

[26] A. Harten, P. Lax et V. Leer, «Upstream differencing and Godunov-type scheme for hyperbolic conservation laws, Upwind and High-Resolution Schemes,» *SIAM Review,* pp. 53-79, 1982.

[27] E. S. D. G. MACIEL, «A Review of some Numerical Methods to the Euler Equation in Two-dimensions,» *WSEAS TRANSACTION on FLUIDS MECHANICS,* vol. 7, n° %13, pp. 81-95, 2012.

[28] C. Parés, «Numerical methods for nonconservative hyperbolic systems : a theoretical framework,» *SIAM Journal on Numerical Analysis,* vol. 44, p. 300–321, 2006.

[29] G. Dal Maso, P. G. Lefloch et F. Murrat, «Defintion and weak stability of nonconservative products,» *J. Math. Pures Appl.,* vol. 74, pp. 483-548, 1995.

[30] A. S. Kleiton, M. G. José, S. B. Dinshaw, N. Boniface et P. Carlos, «Multidimensional approximate Riemann solvers for hyperbolic nonconservative systems. Applications to shallow water systems,» *Journal of Computational Physics ,* vol. 444, p. 110547, 2021.

[31] M. Castro Diaz, A. Kurganov et d. L. Morales, «PATH-CONSERVATIVE CENTRAL-UPWIND SCHEMES FOR NONCONSERVATIVE HYPERBOLIC SYSTEMS,» *ESAIM: Mathematical*

Modelling and Numerical Analysis, vol. 53, pp. 959-985, 2019.

[32] N. A. R. Ngatcha, B. Nkonga, A. Njifenjou et R. Onguene, «Sediment transport models generalized shear shallow water equations,» chez *Conference Africaine pour la Recherche en Informatique et en mathematiques (CARI)*, Dschang (Cameroon) and Tunis (Tunisia), 2022.

[33] M. Dumbser et S. B. Dinshaw, «A New Efficient Formulation of the HLLEM Riemann Solver for General Conservative and Non-conservative Hyperbolic Systems,» *Journal of Computational Physics,* vol. 304, pp. 275-319, 2016.

[34] L. Xin, «A new well-balanced finite volume scheme on unstructured triangular grids for two-dimensional two-layer shallow water flows with wet-dry fronts,» *Journal of computational physics,* vol. 438 , p. 110380, 2021.

[35] S. Cordier, M. Le et T. Morales de Luna, «Bedload transport in shallow water models: Why splitting (may) fail, how hyperbolicity (can) help.,» *Advances in Water Resources,* vol. 34 (8), p. 980{989, 2011.

[36] E. F. Toro, A. Santaca, G. I. Montecinos et L. O. Muller, «AENO: a novel reconstruction method in conjunction with ADER schemes for hyperbolic equations.,» *Communications on Applied Mathematics and Computation.,* 2021.

[37] A. Chertock, S. Cui, A. Kurganov et T. Wu, «Well-balanced positivity preserving central-upwind scheme for the shallow water system with friction terms,» *INTERNATIONAL JOURNAL FOR NUMERICAL METHODS IN FLUIDS,* vol. 78, pp. 355-383, 2015.

[38] D. Marchis et E. Napoli, «3D Numerical Simulation of Curved Open Channel flows,» chez *ASME/WSEAS. Int Conf on Water ressources, Hydraulics&Hydrology*, Chalkida, Greece,, May 11-13, 2006.

[39] A. Kurganov et Tadmor, «New high resolution central-schemes for nonlinear conservation laws and convection-diffusion equations,» *Journal of Computational physics,* vol. 160, pp. 241-282, 2000.

Contribution of Individual Authors to the Creation of a Scientific Article (Ghostwriting Policy)

Conceptualization: Arno Roland Ngatcha.
Data curation: A. Ngatcha and Abdou Njifenjou, Yves Mimbeu
Formal analysis: Arno Roland Ngatcha Ndengna and Abdou Njifenjou, Raphael Onguene
Methodology: Arno Ngatcha and Abdou Njifenjou
Software: Arno Ngatcha
Supervision: Abdou Njifenjou, Sévérin Nguiya,
Validation and Visualization: Arno Ngatcha, Yves Mimbeu
Writing manuscript draft: Arno Ngatcha, Yves Mimbeu

Sources of Funding for Research Presented in a Scientific Article or Scientific Article Itself

This work has not been funded by any source.

Data availability

The data that support the findings of this study are available on request from the corresponding author.

Conflict of Interests

The authors declare that there is no conflict of interest regarding the publication of this paper.

APPENDIX A: Closure model

The transport mode parameter f_s is given by:

$$f_s = \min\left(1;\ 2.5e^{-Z}\right) \quad \text{(A1)}$$

where $Z = \frac{W_s}{\kappa u_*}$ is the Rouse number and where κ is von Karman number ($\kappa = 0.4$).

$u_* = \sqrt{C_f u^2}$ is the shear stress velocity.

$E[Kg/m^2/s]$ and D are the erosion and deposition given by [22]

$$E = \begin{cases} \varphi(\theta - \theta_{cr,50}) h^{-1} |u|, & \text{if } \theta \geq \theta_{cr,50}, \\ 0, & \text{otherwise;} \end{cases} \quad \text{(A2)}$$

$$D = W_s (1 - C_a)^m C_a$$

The deposition rate of sediments D is almost equal to the vertical flux of particles at the boundary.

For erosion rate, $\theta = \frac{hC_f}{(s-1)d_{50}}$ is the Shields parameter,

$\theta_{cr,50} = \frac{0.3}{(1+1.2D_*)} + 0.055(1 - \exp(-0.02D_*))$ is the critical shields parameter.

D_* is the dimensionless grain size parameter, depending on the submerged specific gravity of sediment.

$\varphi\left[m^{1.2}\right]$ is a coefficient that controls the erosion force (we take $\varphi = 0.015$ it for all the simulations in this paper).

In areas where the current is faster than the reference current, erosion is favored. Conversely, when the forcing is more intense than friction, we speak of deposition. Erosion takes place when $\frac{\vec{q}}{q}.\frac{\nabla q}{q} \succ 0$ and deposition when $\frac{\vec{q}}{q}.\frac{\nabla q}{q} \prec 0$. For sediment deposition, m represent the effect of hindered settling due to high sediment concentration (we take here $m = 2$); W_s is the fall velocity of sediment given by:

$$W_s = \sqrt{\left(\frac{13.95\nu}{d_{50}}\right)^2 + 1.09sgd_{50}} - 13.95\frac{\nu}{d_{50}} \quad \text{(A3)}$$

where ν is the kinematic viscosity of water ($\nu = 1.2\times10^{-6}$), d_{50} is the average diameter of sediment particles, $s = \frac{\rho_s}{\rho_w} - 1$ is the submerged specific gravity of sediment, where ρ_s is the sediment density and ρ_w the water density.

C_a is the local near-bed sediment concentration in volume which can be determined following [5] :

$$C_a = \alpha_c C \quad \text{(A4)}$$

$$\frac{1}{\alpha_c} = \begin{cases} \left|\frac{A(1-A^r)}{r}\right| & \text{if } |Z-1| > 10^{-4} \\ |-A\log(A)| & \text{if } |Z-1| < 10^{-4} \end{cases} \quad \text{(A5)}$$

$$r = \begin{cases} \min(Z-1;3) & \text{if } |Z-1| > 10^{-4} \\ 0 & \text{if } |Z-1| < 10^{-4} \end{cases} \quad \text{(A6)}$$

with $A = \max(\frac{\delta_a}{h}, 1)$, $\delta_a[m]$ being the active layer of the bed which is the height of the bedload zone or active layer. That is:

$$\delta_a = \max(0.007(\tau_b - \tau_{cr})\rho_w, 0) + k_s, \quad \text{(A7)}$$

where $\tau_b\,[N/m^2]$ is the grain-related bed-shear stress given by:

$$\tau_b = \rho_w g \frac{|u|}{C_z^2}, \quad C_z = 5.75\sqrt{g}\ln\left(\frac{12R_h}{k_s}\right), \quad \text{(A8)}$$

$R_h[m]$ is the hydraulic radius, (assumed to be equal to water depth).

The critical bed shear stress τ_{cr} is

$$\tau_{cr} = \theta_{cr}\rho_w g(s-1)d_{50}. \quad \text{(A9)}$$

$k_s[m]$ is a roughness coefficient taking into account the sediment condition supply (see appendix B).

APPENDIX B: Sediment supply condition

Knowledge of the quantity of sediment that can be mobilized on a sedimentary bed can help to improve the performance of existing sediment transport models. Studies on sediment availability are very rare. However, among those that have led to new results, they have yet to be applied to real situations. Sediment availability can influence sediment transport by bedload, the migration speed of sedimentary structures, and the mean current profile. Its impact on the morphodynamics of a sedimentary bed on the movement threshold. The sediment supply impacts sediment transport in the coastal context and plays a role in deposition/transportation processes. The impact of the sediment supply on the morphodynamics of a sedimentary bed subject to a current was experimentally studied in the coastal context by Vah et al [6]. The consideration of this physical

parameter is necessary for a good numerical simulation. Some models describing deposition and erosion should integrate this parameter. Relationships to predict equivalent roughness k_s for oscillatory sheet flow can be computed with or without Shields number. According to Rijn [7] and Taking into account sediment supply conditions. We have:

$$k_s = 3d_{90} + 1.1h_{eq}\left(1 - \exp\left(\frac{-25h_{eq}}{\lambda_{eq}}\right)\right) \quad \text{(B.1)}$$

d_{90} is the grain size where the material is finer (m). h_{eq} is the height (m), and λ_{eq} is the bed form length (m). Taking into account sediment supply conditions, we have:

$$\frac{\lambda_{eq}}{\lambda_{eq\_inf}} = 1 - \beta_T \exp\left(\frac{-\delta}{\gamma_T h_{eq\_inf}}\right). \quad \text{(B.2)}$$

and $$\frac{h_{eq}}{h_{eq\_inf}} = 1 - \beta_T \exp\left(\frac{-\delta}{\alpha_T \theta' h_{eq\_inf}}\right) \quad \text{(B.3)}$$

We take here $\beta_T = 0.48,\ \gamma_T = 0.62$.

$\theta' = \dfrac{u'_*}{(s-1)gd_{50}}$ with u'_* bottom velocity without bedforms and based on grain diameters.

$\alpha_T = 8.24$, θ' is the Shields parameter calculated without bedforms or skin friction Shields parameter.

h_{eq_inf} and λ_{eq_inf} are respectively the height and length at the equilibrium state for unlimited sediment supply conditions we have :

$h_{eq\_inf} = 202 d_{50} D_*^{-0.554}$,

$\lambda_{eq\_inf} = d_{50}\left(500 + 1881 D_*^{-1.5}\right)$ (B.4)

APPENDIX C: Double mesh for decoupled sediment transport model.

It is possible to decouple system (1) into two sub-systems. The first sub-system contains Saint-Venant-Exner equations and the second sub-system contains only the sediment transport equation given by the suspension equation. In this case, the suspension equation is given by

$$\frac{\partial(hC)}{\partial t} + \frac{\partial(huC)}{\partial x} = \frac{\partial}{\partial x}\left(f_s h \nu_m \frac{\partial C}{\partial x}\right) + (E - D)$$

can be solved by the fractional steps method which implies that: $\dfrac{\partial(hC)}{\partial t} + \dfrac{\partial(huC)}{\partial x} = \dfrac{\partial}{\partial x}\left(f_s h \nu_m \dfrac{\partial C}{\partial x}\right)$ (C2.1)

$$\frac{\partial(hC)}{\partial t} = E - D \quad \text{(C2.2)}$$

Eq. (C1.1) is solved using a finite volume method, to find the intermediate solution hC, the initial value problem in (C2.2) is solved to obtain the solution next time.

Eq. (C1.1) can be transformed into an integral one to conserve mass

$$\frac{\partial}{\partial t}\int_{K_i}(hC)dx + \sum(huC) = \sum\left(f_s h \nu_m \frac{\partial C}{\partial x}\right) \quad \text{(C3)}$$

The first term is the unsteady term, the second is the convective term and the RHS term is the diffusive term.

The strategy of discretization consists to consider two different meshes. The first is based on the center cell-centered mesh (red color) and the second is based on the cell vertex-centered mesh (black color). We solve the first subsystem in the first mesh and the sediment transport equation is solved in the second mesh (see Fig. 3).

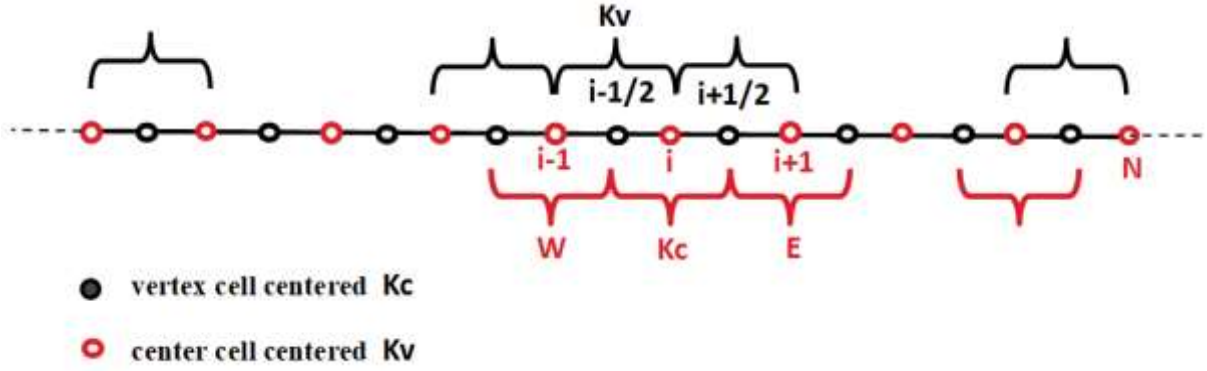

Fig. 3: Finite volume gridding: double meshes for the decoupled sediment transport problems

The grid of each cell is assumed uniform.

The measure of a vertex-centered cell and a cell-centered at the center is denoted by dx_v dx_c and respectively. Here, for simplicity, we assume that $dx = dx_c = dx_v$. In Fig. 3,

W= West, E=East. The cell vertex centered is denoted by $K_v = K_{i+1/2}$ and $K_c = K_i$ denotes the cell center centered. These measures are denoted by $mes(K_{i+1/2})$ $mes(K_i)$ and respectively. The first term is discretized by using an explicit method (or Euler method):

$$\frac{\partial}{\partial t}\int_{K_{i+1/2}} (hC)dx = \frac{C_{i+1/2}^{n+1} - C_{i+1/2}^{n}}{dt} h_i^n \Delta x \quad \text{(C4)}$$

where $C_{i+1/2}^{n+1}$ is an approximation of at vertex cell centered at the time $n+1$, and where dx_V is the measure of the vertex cell centered.

The second term is discretized following the approach given by:

$$\sum (huC) = (huC)_{i+1/2} - (huC)_{i-1/2} \quad \text{(C5)}$$

where $(huC)_{i+1/2}$ is given by:

$$(huC)_{i+1/2} = q_{i+1/2}\left(\frac{C_{i+1}+C_i}{2}\right) - \left|q_{i+1/2}\right|\left(C_{i+1}-C_i\right) \quad \text{(C6)}$$

where $q_{i+1/2}$ is given by AENO reconstruction?

Therefore, the discrete flux is given at second-order accuracy. To get the second order at the time we used the Crank-Nicolson method

$$C_i = \tau C_i^{n+1} + (1-\tau)C_i^n = C_i^n + \tau\left(C_i^{n+1} - C_i^n\right), \quad \text{(C7)}$$

where τ is the positive parameter ($0 \le \tau \le 1$) The final convective scheme is given by (C8):

$$\begin{aligned}&\left((1-\tau)\left(\frac{q_{i+1/2}}{2}+\left|q_{i+1/2}\right|\right) - \tau\left(\frac{-q_{i-1/2}}{2}+\left|q_{i-1/2}\right|\right)\right)C_i^n - \tau\left(\frac{q_{i+1/2}}{2}+\left|q_{i+1/2}\right|\right)C_{i+1}^n + (1-\tau)\left(\frac{-q_{i-1/2}}{2}+\left|q_{i-1/2}\right|\right)C_{i-1}^n \\ &+(1-\tau)\left(\frac{q_{i+1/2}}{2}+\left|q_{i+1/2}\right|\right)C_{i+1}^{n+1} - \tau\left(\frac{q_{i+1/2}}{2}+\left|q_{i+1/2}\right|\right)C_i^{n+1} + (1-\tau)\left(\frac{-q_{i-1/2}}{2}+\left|q_{i-1/2}\right|\right)C_i^{n+1} - \tau\left(\frac{-q_{i-1/2}}{2}+\left|q_{i-1/2}\right|\right)C_{i-1}^{n+1}\end{aligned} \quad \text{(C8)}$$

Diffusive term

To find the second-order accurate discrete scheme, we use the central differential and Crank-Nicolson method.

$$\sum\left(f_s h \nu_m \frac{\partial C}{\partial x}\right) = \left(\nu_m\left(f_{s,i+1/2}h_{i+1/2}^{-}\frac{C_{i+1}-C_i}{\Delta x} - f_{s,i-1/2}h_{i-1/2}^{+}\frac{C_i - C_{i-1}}{\Delta x}\right)\right) \quad \text{(C9)}$$

Using Eq. (41), we obtain

$$\sum\left(f_s h \nu_m \frac{\partial C}{\partial x}\right) = \tau\left(\mu_1 C_i^{n+1} + \mu_2 C_{i+1}^{n+1} + \mu_3 C_{i-1}^{n+1}\right) + (1-\tau)\left(\mu_1 C_i^n + \mu_2 C_{i+1}^n + \mu_3 C_{i-1}^n\right) \quad \text{(C10)}$$

where

$$\mu_1 = \frac{\left(\nu_{s,i+1/2}h_{i+1/2} + \nu_{s,i-1/2}h_{i-1/2}\right)}{\Delta x},\ \mu_2 = \frac{\left(\nu_{s,i+1/2}h_{i+1/2}\right)}{\Delta x},\ \mu_3 = \frac{\left(\nu_{s,i-1/2}h_{i-1/2}\right)}{\Delta x} \quad \text{(C11)}$$

The final fully second-order scheme for the sediment concentration equation is given by:

$$\left(\left(1-\tau\right)\left(\frac{q_{i+1/2}}{2}+\left|q_{i+1/2}\right|\right)-\tau\left(\frac{-q_{i-1/2}}{2}+\left|q_{i-1/2}\right|\right)\right)C_i^n-\tau\left(\frac{q_{i+1/2}}{2}+\left|q_{i+1/2}\right|\right)C_{i+1}^n+\left(1-\tau\right)\left(\frac{-q_{i-1/2}}{2}+\left|q_{i-1/2}\right|\right)C_{i-1}^n$$
$$+\left(1-\tau\right)\left(\frac{q_{i+1/2}}{2}+\left|q_{i+1/2}\right|\right)C_{i+1}^{n+1}-\tau\left(\frac{q_{i+1/2}}{2}+\left|q_{i+1/2}\right|\right)C_i^{n+1}+\left(1-\tau\right)\left(\frac{-q_{i-1/2}}{2}+\left|q_{i-1/2}\right|\right)C_i^{n+1}-\tau\left(\frac{-q_{i-1/2}}{2}+\left|q_{i-1/2}\right|\right)C_{i-1}^{n+1}$$
$$\frac{C_i^{n+1}-C_i^n}{dt}h_{i+1/2}dx=\tau\left(\mu_1C_i^{n+1}+\mu_2C_{i+1}^{n+1}+\mu_3C_{i-1}^{n+1}\right)+\left(1-\tau\right)\left(\mu_1C_i^n+\mu_2C_{i+1}^n+\mu_3C_{i-1}^n\right) \tag{C12}$$

The fully discrete scheme given by Eq. (C12) permits obtaining C_i^{n+1} an intermediate solution. The solution of system (C2) $C_{*,i}^{n+1}$ is obtained by solving Eq. (C2.2) by the third-order semi-implicit Runge-Kutta (SI-RK3) as in [37] (see also [14]).